

REGULAR PAPER

Graphitic cage transformation by electron-beam-induced catalysis with alkali-halide nanocrystals

To cite this article: Jun-ichi Fujita *et al* 2016 *Jpn. J. Appl. Phys.* **55** 055102

View the [article online](#) for updates and enhancements.

You may also like

- [Surface charge dependent structure of ionic liquid/alkali halide interfaces investigated by atomic force microscopy](#)
Harshal P. Mungse, Saki Okudaira, Miho Yamauchi *et al.*
- [Halogen vacancy migration at surfaces of CsPbBr₃ perovskites: insights from density functional theory](#)
R-I Biega and L Leppert
- [Electronic properties and degradation upon VUV irradiation of sodium chloride on Ag\(111\) studied by photoelectron spectroscopy](#)
Haibo Wang, Martin Oehzelt, Stefanie Winkler *et al.*



Graphitic cage transformation by electron-beam-induced catalysis with alkali-halide nanocrystals

Jun-ichi Fujita^{1,2*}, Masashi Tachi^{1,2}, Naoto Ito^{1,2}, Katsuhisa Murakami^{1,2}, and Masaki Takeguchi³

¹*Institute of Applied Physics, Graduate School of Pure and Applied Sciences, University of Tsukuba, Tsukuba, Ibaraki 305-8573, Japan*

²*Tsukuba Research Center for Interdisciplinary Materials Science, University of Tsukuba, Tsukuba, Ibaraki 305-8573, Japan*

³*National Institute for Materials Science, Tsukuba, Ibaraki 305-0047, Japan*

*E-mail: fujita@bk.tsukuba.ac.jp

Received November 21, 2015; accepted February 19, 2016; published online April 12, 2016

We found that alkali-halide nanocrystals, such as KCl and NaCl, have strong catalytic capability to form graphitic carbon cages from amorphous carbon shells under electron beam irradiation. In addition to the electron beam irradiation strongly inducing the decomposition of alkali-halide nanocrystals, graphene fragments were formed and linked together to form the final product of thin graphitic carbon cages after the evaporation of alkali-halide nanocrystals. The required electron dose was approximately 1 to 20 C/cm² at 120 keV at room temperature, which was about two orders of magnitude smaller than that required for conventional beam-induced graphitization. The “knock-on” effect of primary electrons strongly induced the decomposition of the alkali-halide crystal inside the amorphous carbon shell. However, the strong ionic cohesion quickly reformed the crystal into thin layers inside the amorphous shell. The bond excitation induced by the electron beam irradiation seemed to enhance strongly the graphitization at the interface between the outer amorphous carbon shell and the inner alkali-halide crystal.

© 2016 The Japan Society of Applied Physics

1. Introduction

Graphitic carbon cages have potential use for forming the framework of molecular devices, where the curved surface of the graphitic cage effectively produces an electric polarization resulting from a particular deviation of the π -electron density between the inside and outside of the cage.¹⁾ The adoption of phenyl butyric acid methyl ester (PCBM) for the C60 molecule leads to n-type conduction, making the PCBM molecule a candidate material for organic semiconductor devices.^{2,3)} In addition, the local electron and/or spin polarization on the graphitic cage, which would be strongly enhanced by an encapsulated metal, can provide significant functionality for molecular switching devices.^{4,5)} There is a high demand for the artificial control of these carbon-cage structures,^{6,7)} including their size and shape, to enable molecular device applications.

The primary production method for fullerenes and their allotropes is via the arc-plasma method, where the source graphite rods are decomposed at an extremely high temperature of about 3000 K.⁸⁾ Small clusters of carbon atoms and small graphitic fragments coalesce to form fullerenes, in accordance with the “pentagon road”^{9,10)} and “ring coalescence”^{11,12)} models. The non-equilibrium environment produces carbon cages of various sizes, but the production is optimized in terms of the maximum yield of the smallest molecule, C60.

Electron-beam-induced cage transformation has been extensively investigated using in situ transmission electron microscopy techniques.^{13–22)} Static Joule heating under extensive electron dose with the assistance of the “knock-on” process^{23–25)} seems to induce dynamic edge deformations, such as the curling up of the graphene edge and zipping up of the nearest stack of graphene, resulting in the formation of fullerene molecules. Mild activation, such as periodic pulse current injection into the graphite edge,⁷⁾ is crucial for promoting the transformation of larger graphitic carbon cages. Such transformation is achieved through a balance between the attractive van der Waals force on the basal plane and the cyclic stress, which induces curling deformation.

We found that electron beam irradiation of alkali-halide nanocrystals having a thin amorphous carbon shell induced a graphitic cage transformation that inherited the size and shape of the original alkali-halide nanocrystal. The formation of graphene and carbon nanotubes under thermal equilibrium reaction conditions is commonly triggered by dissolved carbon in a seed catalyst such as the transition metals of Fe and Ni. However, carbon is insoluble in alkali halides such as KCl and NaCl, except in the case of producing graphitic fragments from molten sodium with an aerogel-like carbon source.²⁶⁾ Our findings suggest that the crystal surface of alkali-halides seems to have a high catalyzing capability and the decomposition of the crystal results in the formation of hollow graphitic carbon cages.

2. Experimental methods

Nanocrystalline alkali-halides KCl and NaCl supported on carbon mesh grids were the starting materials for the electron-beam-induced graphitic cage transformation. We prepared 0.2 mol/L solutions of KCl and NaCl with distilled water. The solutions were dropped onto carbon mesh grids (Nisshin EM) and dried under atmospheric conditions. The carbon mesh grids were treated with 100 W oxygen plasma for 30 s at approximately 10² Pa of O₂ ambient before preparing the specimens. This process effectively improves the surface wettability, which results in the uniform and thin spreading of the solution on the mesh and the production of alkali-halide nanocrystals.

Specimens were analyzed by scanning electron microscopy (SEM; Hitachi S4800) and transmission electron microscopy (TEM; JEOL JEM-9200 and JEM-ARM200F). The source of the amorphous carbon for the graphitic cages was the natural carbon contamination that is deposited on the nanocrystals during SEM beam irradiation. The background pressure in the SEM specimen chamber was kept below 10⁻³ Pa during beam operation. Typically, 1 nm of amorphous carbon was deposited at an electron dose of approximately 40 mC/cm² at 5 keV.

The emission current in TEMs was evaluated from the current density that was measured on a fluorescent plate of

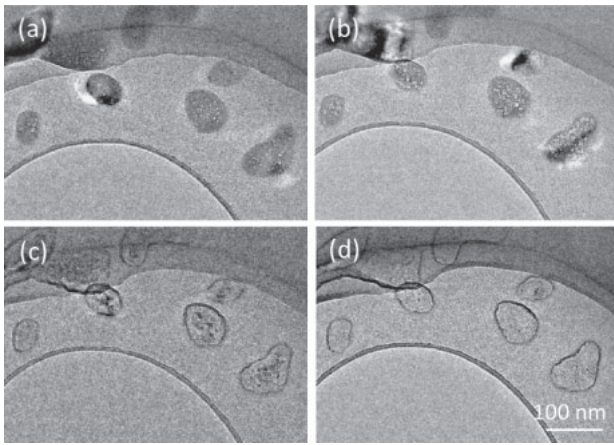


Fig. 1. TEM images of a typical transformation sequence for a KCl nanocrystal. The KCl nanocrystals showed crystallinity, demonstrated by the following image sequence. (a) Dark contrast observed in the bright-field image (Bragg diffraction), (b) dynamic fluctuations of the dark contrast give the appearance of intense blinking, (c) the dark contrast becomes brighter as a hollow space is formed inside the nanocrystal, and (d) a few layers of the graphitic carbon cage, which had the size and shape of the initial nanocrystal, were produced.

200 cm² size, and the beam current was adjusted to be typically in the range from 2 to 10 nA. The electron current density in the specimen increased with the inverse square of magnification power, where the typical electron dose was 17 C/cm² at 60,000 magnification power and a beam current of 3.2 nA for 300 s beam irradiation, and the beam current density was approximately 60 mA/cm² in the specimen.

3. Results and discussion

3.1 Transformation sequence

Figure 1 shows the typical transformation sequence from a surrounding amorphous carbon to a graphitic carbon cage for a KCl nanocrystal induced with a 120 keV primary electron beam. The high crystallinity of the KCl nanocrystal produced a dark contrast in the bright-field image. The spherical aberration of the objective lens generated some of the bright ghost spots, which result from the Bragg diffraction around the dark contrast of the nanocrystal, as shown in Fig. 1(a). After 30 s of beam irradiation, the intensities of the dark contrast and the bright spots fluctuated dynamically, generating the appearance of intense blinking, as shown in Fig. 1(b) (see Fig. S1 and movie in the online supplementary data at <http://stacks.iop.org/JJAP/55/055102/mmedia>). The dark contrast of the nanocrystals became brighter, which indicates the formation of a hollow space inside the nanocrystal that contains fragments of the nanocrystals, and the graphitic cage became clearly visible after 60 s of beam irradiation, as shown in Fig. 1(c). Finally, the dark contrast of the nanocrystal disappeared, and clear dark fringes appeared after 300 s of beam irradiation, as shown in Fig. 1(d). The required electron dose for the complete removal of the KCl nanocrystal was approximately 17 C/cm² at 120 keV and room temperature, but the minimum electron dose for creating the graphitic cage would be much smaller than about 3 C/cm², as determined from Fig. 1(c).

However, the electron dose for the complete transformation sensitively depended on the size of the alkali-halide nanocrystal and the thickness of the surrounding amorphous

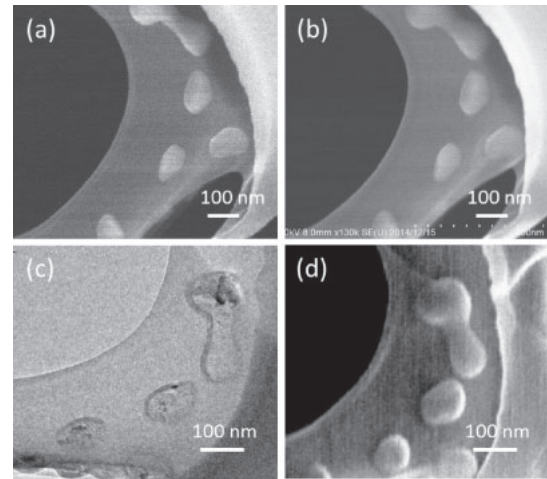


Fig. 2. (a) SEM images of the cage formation process of initial KCl nanocrystals adhering to a carbon mesh, (b) SEM image taken immediately after carbon contamination deposition, (c) TEM image after cage transformation, and (d) SEM image corresponding to (c).

carbon; the required electron dose seemed to decrease to be nearly proportional to the top area of the nanocrystals rather than the volume. The electron penetration depth at 120 keV would be approximately 100 μm for an alkali-halide medium of 2.1 g/cm², which was much larger than the thickness of the KCl and NaCl nanocrystals. Thus, decomposition of the nanocrystals could uniformly proceed inside the crystal body. However, chlorine was desorbed from the outermost surface thus, the required electron dose would be proportional to the square of crystal size (top surface area). Thicker surrounding amorphous carbon also suppressed the escape of chlorine and the alkali metal from the amorphous carbon shell. Thus, the minimum electron dose for the cage transformation would be decreased to be approximately 1 C/cm² for a small alkali-halide nanocrystal with a thin amorphous carbon shell.

The dark fringes observed in Fig. 1(d) suggests the existence of five to seven layers of graphitic basal planes parallel to the beam incident azimuth, having almost the same size and shape as the original nanocrystal. SEM images verified the exact form of the semispherical three-dimensional cage structure.

The transformation sequence taken from the same area of the specimen is shown in Fig. 2, where Fig. 2(a) shows an SEM image of the initial KCl nanocrystals on the carbon mesh, and (b) shows an SEM image of the structures immediately after carbon contamination deposition. Although the TEM image (c) taken after the transformation only shows the cross-sectional outline of the cage through the projected image of the cage, the three-dimensional cage structure can be confirmed from the SEM image in (d).

E-beam irradiation decomposed and fragmented the initial block of the KCl nanocrystal. Reduction in the initial volume of the nanocrystals resulted in the creation of a hollow space inside the amorphous carbon shell, accompanied by a dynamic movement of the fragmented crystals inside the shell as shown in Figs. 3(a) and 3(b) (see Fig. S2 and in-situ movie in the online supplementary data at <http://stacks.iop.org/JJAP/55/055102/mmedia>). The cage transformation progresses inside of the amorphous carbon shell. Decomposed chlorine will easily escape through the defects

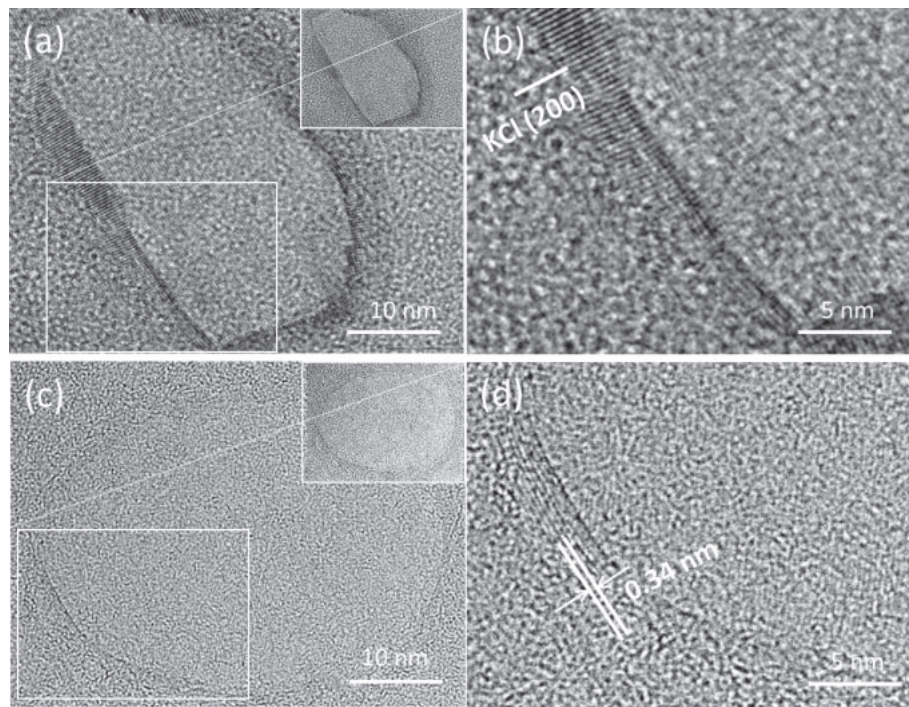


Fig. 3. High-resolution TEM images of intermediate cage transformation. (a) Alkali-halide nanocrystals aggregating at the interface region facing amorphous carbon shell. (b) Enlarged image of the region indicated in (a), showing the KCl(200) planes perpendicular to the shell. (c) Graphitic cage formed after the alkali-halide migrated. (d) Enlarged image of the region indicated in (c), showing that four to five graphitic layers were created.

of the amorphous carbon shell, and also, many pores and boundaries of the uncompleted graphitic cage would be the presumable pathways for chlorine evaporation. Thus, the use of a thicker shell resulted in a longer transformation time.

On the other hand, potassium diffused around the shell, which we confirmed by energy dispersive X-ray spectroscopy (EDS) analysis. However, some of the chlorine and potassium in the shell remain as KCl nanocrystals at the intermediate stage of the transformation. The thin layer of KCl nanocrystals adhering to the inner side of the shell was observed as a faintly appearing square lattice in (b) with a coherent domain area of about 30 to 50 nm. Here, the interfered fringes, identified to be the KCl(200) plane, partially appeared inside the shell, when the beam azimuth was incidentally aligned to the crystal axis of the fragments.

Figures 3(c) and 3(d) show the TEM images after the transformation. The graphitic cage consisting of four to five graphene layers having a 0.34 nm interlayer spacing was formed after the disappearance of alkali-halide nanocrystals. We observed that the intense beam irradiation easily damaged the graphitic cage. However, the alkali-halide immediately migrated and adhered again, as if to reform the graphitic cage. In this case, the “knock-on” effect of the primary electron beam actively induced the decomposition and migration of the alkali-halide nanocrystals inside the amorphous carbon shell. However, the high ionic cohesion soon reforms the thin crystal layers inside the amorphous shell and/or the graphitic cage to reconstruct the graphene layers.

3.2 Transformation model

Figures 4(a) to 4(c) show sequential images of a typical cage structure transformation, and Fig. 4(d) shows a schematic illustration of the transformation. Electron beam irradiation actively induces the decomposition of alkali-halide crystals,

but fragmented nanocrystals are still embedded at the interface of the shell, partially showing lattice images of KCl(200), as shown in Fig. 4(a). Reducing the thickness of the KCl layers under additional electron irradiation gives rise to the faint appearance of graphite 0002 fast Fourier transform (FFT) spots, enclosed in white circles in Fig. 4(b). While the diffraction spots of KCl 200 were elongated in the direction normal to the interface, the lattice spacing was larger than the KCl lattice spacing (0.31 nm) and closer to the bulk graphite lattice spacing (0.34 nm). Thus, the lattice spacing between KCl nanocrystals seemed to widen during the graphitizing reaction immediately before the complete decomposition. Note that the elongation of the FFT spots is the side effect of the area enclosed in the rectangles in Fig. 4(b) for the FFT conversion.

After the transformation, a clear lattice image of the graphitic cage was observed, as shown in Fig. 4(c). The coexistence of small fragments of graphene platelets, as shown in Fig. 4(d), could be the cause of such faint FFT spots in Fig. 4(b), and that the bright graphite 0002 FFT spots appear immediately after the platelet fragments link together.

3.3 Cage transformation with NaCl

Our experiments confirm that NaCl nanocrystals would also be a useful seed material for producing carbon cages through electron-beam-induced reactions. As shown in Fig. 5, the decomposition of NaCl nanocrystals and the formation of graphitic cage structures followed the same route as that of KCl. The major alignment of NaCl nanocrystals had the (200) preferred orientation on the amorphous carbon mesh, coexisting with nanocrystals with (220) alignment. The cage transformation process from NaCl nanocrystals is as follows: the dark contrast of NaCl nanocrystals accompanying bright Bragg diffraction spots dynamically fluctuated [Fig. 5(a)],

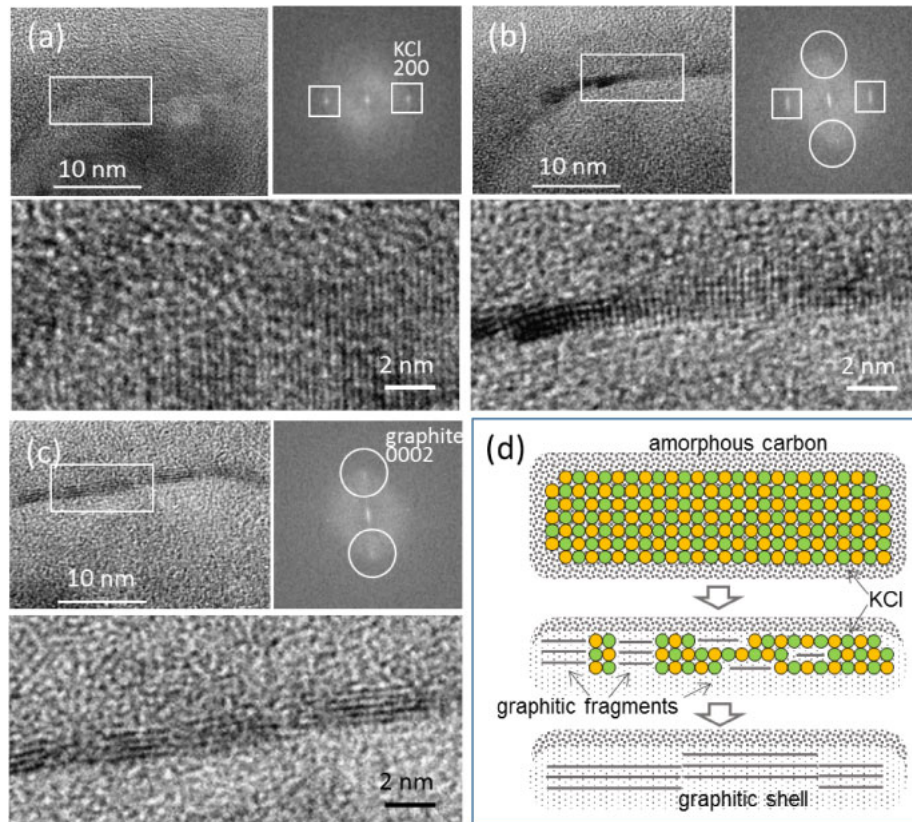


Fig. 4. (Color online) TEM images of the cage structure transformation. (a) A KCl nanocrystal encapsulated in the carbon shell shows the characteristic lattice of the KCl(200) plane. (b) Electron beam irradiation reduces the KCl thickness and weak graphene 0002 spots appear. (c) A clear lattice image of graphene. (d) Schematic of cage transformation sequence.

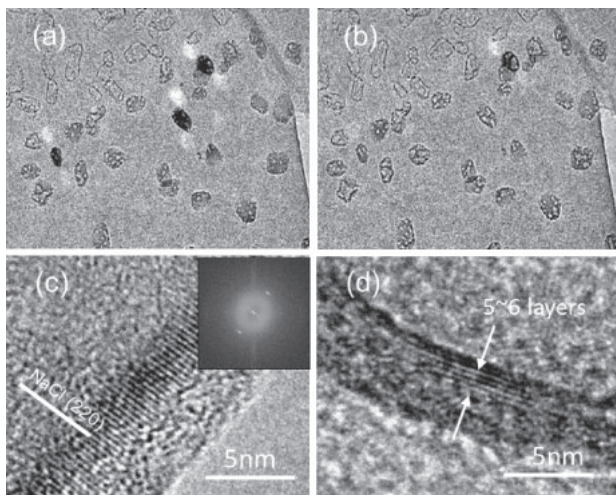


Fig. 5. Transformation sequence of NaCl nanocrystal. (a) TEM image before e-beam irradiation. (b) Intermediate state during beam irradiation. (c) NaCl(220) crystal planes appear perpendicular to the outer amorphous carbon shell. (d) Graphitic carbon cages were produced.

and the deposited amorphous carbon on the NaCl nanocrystals finally transformed into graphitic carbon cages [Fig. 5(b)]. The required electron dose for the cage transformation from NaCl nanocrystals was approximately 10 C/cm^2 at 120 keV for this specimen, which is almost the same as that required for the cage transformation with KCl. The multiple repetitions of the decomposition and the recombination of Na and Cl atoms finally generated a thin NaCl layer embedded inside the amorphous carbon shell, and the

interfered lattices of the (200) and (220) planes frequently appeared [Fig. 5(c)], immediately before the graphitic cage was formed [Fig. 5(d)].

The coverage of the amorphous carbon shell was crucial to realizing the cage transformation shown in Fig. 6. The bare NaCl nanocrystal supported on the carbon membrane is easily decomposed, and the NaCl crystal structure disappeared at an electron dose of 1 C/cm^2 , as shown in Fig. 6(c). The energy-dispersive X-ray spectroscopy (EDS) analysis that was carried out on the same specimen area of the TEM image suggests that the Na atoms widely and uniformly migrated on the carbon mesh, as shown in Fig. 6(e), but the low count of chlorine on the mesh surface suggests that chlorine evaporated into vacuum during e-beam irradiation.²⁵ Therefore, encapsulation with amorphous carbon plays an essential role in sustaining the catalysis for forming a graphitic shell. However, thicker encapsulation reduced both the desorption and migration rates of alkali-halide nanocrystals, thus, the reaction for the cage transformation required a much longer time, resulting in an apparent large electron dose.

4. Discussion

Graphitic onion formation has been observed by TEM with an intense electron beam irradiation of 900 A/cm^2 for 25 min,¹⁵ which is identical to the electron dose of $1 \times 10^6 \text{ C/cm}^2$. Thus, such a nonequilibrium condition produced by the intense electron bombardment significantly contributed to the onion cage transformation. Some reports predicted that these transformations were triggered by beam irradiation at

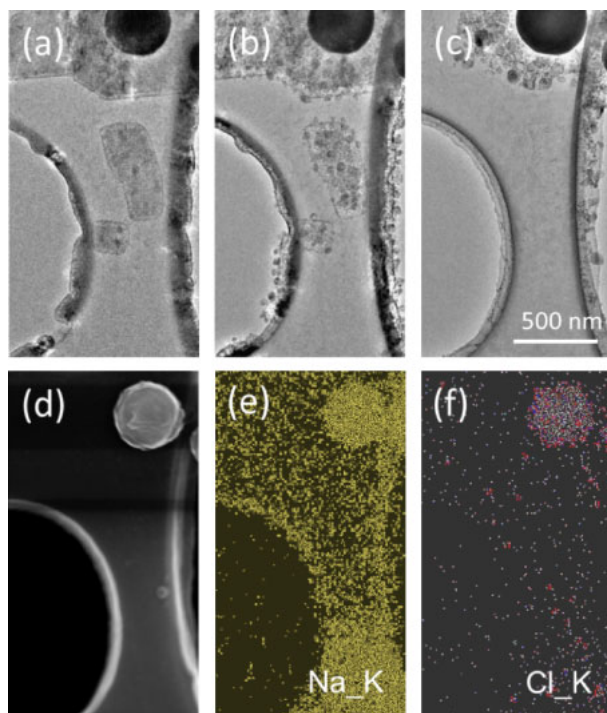


Fig. 6. (Color online) Transformation sequence of NaCl nanocrystal without amorphous carbon coverage: (a) TEM image at the start of beam irradiation, (b) intermediate stage of the decomposition of NaCl nanocrystals, and (c) NaCl nanocrystals disappeared at an accumulated electron dose of 1.0 C/cm^2 . The SEM image in (d) shows the EDS analysis area that was identical to the TEM image in (c). The EDS map (e) suggests that sodium was uniformly dispersed on the carbon mesh, but (f) chlorine was desorbed into vacuum.

current densities exceeding 100 A/cm^2 for 3–5 min ($1 \times 10^4\text{ C/cm}^2$)^{13,16} in combination with a specimen temperature of approximately 700 K. The electron beam current density for high-resolution imaging was typically in the range of 1 to 50 A/cm^2 at a magnification power of approximately 600,000, and the maximum current density attainable with conventional TEM would be $\sim 500\text{ A/cm}^2$. In contrast, our cage transformation process was observed at a relative low magnification power, in the range of 10000 to 60000. Thus, the current density was reduced to 60 mA/cm^2 , and the interfacial graphitic cage transformation observed here requires current density of approximately 1 to 20 C/cm^2 , which is about two to four orders of magnitude less than that necessary for the graphitic cage transformation of amorphous carbon without a metal catalyst. Although the electron bombardment, as well as the Joule heating effect, should be incorporated in the graphitizing reaction, we consider that this remarkable electron dose reduction indicates that the alkali-halide nanocrystals have a catalytic capability mediated by the electron-beam-induced reaction.

Other examples of alkali-metal-induced graphitization have been reported. An aerogel-like carbon was graphitized in molten sodium at $800\text{ }^\circ\text{C}$ under ambient atmospheric conditions²⁷ and Cs in the vapor phase appeared to induce the graphitization of nanoporous carbon.^{28,29} In contrast, potassium has a relatively high adsorption energy (E_a), which is defined as the difference between the energy of a relaxed adatom and graphene, of about 1 eV.^{30,31} If the ratio of E_a to the bulk cohesive energy E_c exceeded unity, then potassium tended to form two-dimensional crystals on the graphitic

surface. This theory suggests that the particular KCl crystal lattice image provides the reasonable representation of the wetting behavior of the KCl crystal inside the shell. The two-dimensional uniform and precision wetting behavior of the alkali metal could induce a significant charge transfer from the graphene layer;³¹ thus, the C–C bond excitation in graphene and amorphous carbon at a very high electron dose would strongly promote the interfacial graphitization of alkali halides. The formation of alkali-halide nanocrystals would actively contribute to the anchoring of the alkali metals above the graphitizing surface.

However, electron energy loss spectroscopy (EELS) suggested that no chemical shift of π^* at 285 eV during the transformation process was observed. Thus, a static and specific chemical bond between carbon and KCl seemed to be not formed during the transformation (see Fig. S3 in the online supplementary data at <http://stacks.iop.org/JJAP/55/055102/mmedia>). However, EELS could not detect such an excited bonding state when the lifetime was very short. We need further investigation for the chemical bonding state of carbon during the transformation.

5. Conclusions

We found that electron beam irradiation of alkali-halide nanocrystals with amorphous carbon shells induced the transformation of amorphous carbon into graphitic carbon cages. The threshold electron dose was typically in the range of 1 to 20 C/cm^2 at a beam energy of 120 keV. The knock-on effect of the primary electrons strongly induced the decomposition of alkali-halide nanocrystals inside the amorphous carbon shell. However, the high ionic cohesion quickly reformed the crystals into thin layers inside the amorphous shell. The bond excitation induced by the electron beam irradiation seemed to enhance the graphitization sharply at the interface between the outer amorphous carbon shell and the inner alkali halide nanocrystals.

Our results demonstrate that alkali-halide nanocrystals triggered the graphitic cage transformation and that the cage has almost the same shape and size as the original nanocrystals. This catalyzing process suggests that connected crystals can produce an elongated tubular cage, which would be very useful as a functional bone structure. Further study is necessary to gain a detailed understanding of the cage transformation mechanism. We believe that this bottom-up process based on the beam-induced alkali-halide crystal reaction, would be a promising method to produce functional carbon cages for future electronic device applications.

Acknowledgments

This work was supported by JSPS KAKENHI Grant Numbers 26107506 and 15H02195. Part of this work was supported by the NIMS microstructural characterization platform (NMCP) as a program of “Nanotechnology Platform” of the Ministry of Education, Culture, Sports, Science and Technology, Japan (MEXT).

- 1) R. C. Haddon, R. E. Palmer, H. W. Kroto, and P. A. Sermon, *Philos. Trans. R. Soc. A* **343**, 53 (1993).
- 2) D. M. Guldi, B. M. Illescas, C. M. Atienza, M. Wielopolskia, and N. Martín, *Chem. Soc. Rev.* **38**, 1587 (2009).

- 3) E. Lörtscher, V. Geskin, B. Gotsmann, J. Fock, J. K. Sørensen, T. Bjørnholm, J. Cornil, H. S. J. van der Zant, and H. Riel, *Small* **9**, 209 (2013).
- 4) L. Liu, S. Liu, X. Chen, C. Li, J. Ling, X. Liu, Y. Cai, and L. Wang, *Sci. Rep.* **3**, 3062 (2013).
- 5) S. Vijayaraghavan, D. Écija, W. Auwärter, S. Joshi, K. Seufert, A. P. Seitsonen, K. Tashiro, and J. V. Barth, *Nano Lett.* **12**, 4077 (2012).
- 6) A. V. Krasheninnikov and F. Banhart, *Nat. Mater.* **6**, 723 (2007).
- 7) T. Nishijima, R. Ueki, E. Kano, and J. Fujita, *Jpn. J. Appl. Phys.* **51**, 06FD20 (2012).
- 8) W. Krätschmer, L. D. Lamb, K. Fostiropoulos, and D. R. Huffman, *Nature* **347**, 354 (1990).
- 9) N. S. Goroff, *Acc. Chem. Res.* **29**, 77 (1996).
- 10) H. W. Kroto and K. McKay, *Nature* **331**, 328 (1988).
- 11) J. M. Hunter, J. L. Fye, E. J. Roskamp, and M. F. Jarrold, *J. Phys. Chem.* **98**, 1810 (1994).
- 12) Y. Rubin, M. Kahr, C. B. Knobler, F. Diederich, and C. L. Wilkins, *J. Am. Chem. Soc.* **113**, 495 (1991).
- 13) F. Banhart, *Rep. Prog. Phys.* **62**, 1181 (1999).
- 14) C. Kiang, W. A. Goddard, III, R. Beyers, and D. S. Bethune, *J. Phys. Chem.* **100**, 3749 (1996).
- 15) G. Lulli, A. Parisini, and G. Mattei, *Ultramicroscopy* **60**, 187 (1995).
- 16) J. Y. Huang, *Nano Lett.* **7**, 2335 (2007).
- 17) T. Oku, G. Schmid, and K. Suganuma, *J. Mater. Chem.* **8**, 2113 (1998).
- 18) T. Füller and F. Banhart, *Chem. Phys. Lett.* **254**, 372 (1996).
- 19) C. Jin, K. Suenaga, and S. Iijima, *J. Phys. Chem. C* **113**, 5043 (2009).
- 20) J. Fujita, M. Tachi, K. Murakami, H. Sakurai, Y. Morita, S. Higashibayashi, and M. Takeguchi, *Appl. Phys. Lett.* **104**, 043107 (2014).
- 21) M. Takeuchi, S. Muto, T. Tanabe, S. Arai, and T. Kuroyanagi, *Philos. Mag.* **76**, 691 (1997).
- 22) K. Mølhave, S. B. Gudnason, A. T. Pedersen, C. H. Clausen, A. Horsewell, and P. Bøggild, *Ultramicroscopy* **108**, 52 (2007).
- 23) B. W. Smith and D. E. Luzzia, *J. Appl. Phys.* **90**, 3509 (2001).
- 24) A. Zobelli, A. Gloter, C. P. Ewels, G. Seifert, and C. Colliex, *Phys. Rev. B* **75**, 245402 (2007).
- 25) I. Ohnishi, K. Shibuya, K. Tachibana, J. Yamagata, M. Morita, T. Watanabe, S. Miyazawa, H. Takahashi, Y. Ohkura, and Y. Kondo, *Microsc. Microanal.* **18**, 1052 (2012).
- 26) J. H. Warner, M. H. Rummeli, L. Ge, T. Gemming, B. Montanari, N. M. Harrison, B. Buchner, and G. A. D. Briggs, *Nat. Nanotechnol.* **4**, 500 (2009).
- 27) Z. J. Xu, B. Z. Xia, W. Y. Wang, T. Ji, C. Ma, and L. H. Gan, *Carbon* **49**, 3385 (2011).
- 28) E. R. Margine, A. N. Kolmogorov, D. Stojkovic, J. O. Sofo, and V. H. Crespi, *Phys. Rev. B* **76**, 115436 (2007).
- 29) K. W. McNamara, P. Ayyappan, R. Rajagopalan, J. G. Chen, and H. C. Foley, *Carbon* **56**, 109 (2013).
- 30) X. Liu, C. Z. Wang, M. Hupalo, W. C. Lu, M. C. Tringides, Y. X. Yao, and K. M. Ho, *Phys. Chem. Chem. Phys.* **14**, 9157 (2012).
- 31) X. Liu, C. Z. Wang, M. Hupalo, H. Q. Lin, K. M. Ho, and M. C. Tringides, *Crystals* **3**, 79 (2013).